Atmospheric Pollution Research
www.atmospolres.com

Remote sensing of desert dust over Kuwait: long–term variation

Ismail Sabbah [1,2], Humood F. Al–Mudhaf [3], Abdullah Al–Kandari [4], Faisal Al–Sharifi [5]

[1] *Department of Natural Sciences, College of Health Sciences, Public Authority of Applied Education and Training, Kuwait*
[2] *Department of Physics, Faculty of Science, Alexandria University, Alexandria, Egypt*
[3] *Department of Chemical Engineering, College of Technological Studies, Public Authority of Applied Education and Training, Kuwait*
[4] *Department of Curriculum and Instruction, College of Basic Education, Public Authority of Applied Education and Training, Kuwait*
[5] *Department of Environmental Sciences, College of Health Sciences, Public Authority of Applied Education and Training, Kuwait*

ABSTRACT

Aerosol optical measurements acquired with satellite–borne TERRA/Moderate Resolution Imaging Spectro–radiometer (MODIS) sensor were analyzed over Kuwait. The study focuses on the seasonal variation of aerosol optical thickness (AOT) and their relationship with meteorological parameters during the 7–year period from 2000 through 2007. The mean values of AOT, wind speed (V), air temperatures (T), diurnal temperature range (ΔT) and water vapor content (WVC) in the near-infrared (NIR) region were high during spring (April–May), while those of the Angstrom wavelength exponent α were low. These low values of α indicate the presence of large aerosol particles (dust). Spectral analysis shows a significant annual variation in the AOT and meteorological parameters. The second (semi–annual), third (4–month) and fourth (3–month) harmonics of the annual variation are also evident. The fourth harmonic is well defined in WVC (NIR) spectra. The power spectral densities of the exponent α, ΔT and RH have a similar spectral power ~1.9. The cross–correlation functions between the time series of the wavelength exponent and each of the meteorological parameters exhibit annual and biennial cycles. The atmosphere over Kuwait is relatively dust free 3 months after WVC (NIR) peaks.

Keywords:
Aerosol optical thickness
Angstrom wavelength exponent
Wind speed
Cross–correlation
Power spectral density
MODIS

Article History:
Received: 25 June 2011
Revised: 29 August 2011
Accepted: 07 October 2011

Corresponding Author:
Ismail Sabbah
Tel: +965-24836577
Fax: +965-24825196
E-mail: sabbahsom@yahoo.com

doi: 10.5094/APR.2012.009

1. Introduction

Aerosols are one of the greatest sources of uncertainty in climate modeling, affecting the radiation budget and cloud processes of the atmosphere. Dust exerts a large influence over radiative transfer processes: directly through scattering and absorbing processes and indirectly by affecting microphysical properties and lifetime of clouds (Andreae, 2001). Tropospheric aerosols significantly influence global climate, by changing the radiative energy balance (Hignett et al., 1999; Haywood and Boucher, 2000; Jacobson 2001; Ghan et al., 2001; Yu et al., 2006) and clouds as well as the hydrological cycle (Rosenfeld, 2000; Ramanathan et al., 2001). Sabbah et al. (2001) measured AOT in Alexandria, Egypt, over a period of 12 months, which included the period of Khamaseen storms that usually blow over Egypt in March. They performed wind trajectory analysis on the Khamaseen period, and in conjunction with the measured AOT, they showed that the presence of dust was associated with air masses movement coming primarily from North Africa. Prospero and Carlson (1972) showed that aircraft measurements indicate that the highest dust concentrations are typically found within the middle–level easterly jet near the southern edge of the Saharan air layer. Although July generally represents a dust free month, Alpert et al. (2002) found dust outbreak during July, 2000 in the Southeastern Mediterranean region. They suggested that a strong dry convection that may have developed over the Saharan source regions may have lifted the dust to a high altitude (above ~700 hPa), thereby allowing the upper–level southwesterly winds to transport the dust northeastward over the Southeastern Mediterranean region. This agrees with the findings of Kaskaoutis et al. (2008). Aerosol reduce aesthetic visibility (Malm et al., 1994; Hand et al., 2000; Watson, 2002) and those less than about 2.5 µm in diameter (known as $PM_{2.5}$) can adversely affect human health by being inhaled into lungs (Prospero, 1999; Samet et al., 2000) or accompany disease (Mims et al., 1997). Dust collected in Kuwait in the 1990s was found to cause cellular membrane and DNA damage (Athar et al., 1998). A study involving 850 school children in the United Arab Emirates found an asthma prevalence rate of 13.6% and an allergic prevalence rate of 72.9% and identified dust storm exposure as one of the significant predictors of these illnesses (Bener et al., 1996). Recent research shows that atmospheric mineral dust carries significant amounts of microorganisms, and that these organisms remain viable after long range transport (Prospero et al., 2005). In samples collected during dust events in Mali, 10% of the bacteria identified were animal pathogens, 5% were plant pathogens, and 27% could be characterized as opportunistic human pathogens (Kellogg et al., 2004). This provides a potential explanation for some of the earlier findings on human health effects.

Jones and Christopher (2008) showed that indirect effects of aerosol over the Arabian Sea are a strong function of season, which is a result of the changing aerosol and moisture (humidity) concen–trations during the course of the year. An increase or decrease in *RH* causes changes in their sizes, volume and density, and eventually in the aerosol optical thickness values. This may lead to

observed seasonal variations between AOT–PM relationships (e.g. Xia et al., 2006).

The Arabian Peninsula is one of the most difficult environments in the world to characterize, monitor and for climate models. It is considered as the largest confluences of dust and anthropogenic emissions in the world. Frequent dust storms and high pollution levels are the main features of the region. AOT was first studied in Kuwait using a portable sunphotometer that was provided by the National Aeronautics and Space Administration (NASA) (Sabbah et al., 2006). Redemann et al. (2006) compared tracking photometer data Angstrom exponent to MODIS–TERRA visible (553–855 nm) and found an *rms* difference better than that with MODIS–Aqua. Ulanowski et al. (2010) studied mineral dust over Kuwait and Saudi Arabia. They found that the atmospheric mineral dust is generally accompanied by electrical charging, and the electric field may in some case reach sufficiently high values for dust particle alignment to occur. Sabbah and Hassan (2008) found that the increase in wind speed is related to the increase of the concentration of dust particles during spring over the Solar Village, (Riyadh, Saudi Arabia). Hoff and Christopher (2009) assessed the viability of AOT as a measure of aerosol "column burden" relevant to the needs the air quality community, which range from determining compliance with ambient standards to input for air quality forecasting and tracking of trends.

The purpose of this work is to study long–term variation of aerosol particles suspended in Kuwait's atmosphere in conjunction with the variations in the meteorological parameters. We examine the entire data sets from February 2000 through February 2007 to determine occurrence of periodicities using power spectral analysis. The slopes of the spectra of aerosol and meteorological parameters have been calculated in order to find the similarity between them. The time lag between the time series of aerosol and meteorological parameters have been calculated using the cross–correlation analysis.

2. Observational Data and Site

Kuwait is a subtropical desert located in the Arabian Peninsula. Dust and sand storms form a major feature of this region together with its arid climate (i.e., extreme heat, low humidity and little precipitation) and extreme surface temperature. Dust and sand storms are a persistent problem in Kuwait; they peak in the spring and summer due to the strong north–westerly "Shamal" winds that characterize the weather during the winter–spring seasonal transition. Aerosol optical properties retrieved from MODIS TERRA satellite over land in Kuwait (29.317°N, 48.017°E) are used in this analysis. The MODIS Atmosphere Products Subset Statistics (MAPSS) products (see http://modis-atmos.gsfc.nasa.gov/products_calendar.html) extract the values of the pixel corresponding to the location (29.317°N, 48.017°E) as well as surrounding pixels falling within a 50 x 50 km box centered on the above location, using the spatial–temporal technique of Ichoku et al. (2002). The MAPSS products are for a 50 km box of 10 km retrievals around the above location. The 50 km box is chosen to correspond with an hour of averaging of the Cimel automatic sun tracking photometer time series. The idea in MAPSS is to compare temporal statistics observed by TERRA with spatial statistics observed by the ground sun photometer rather than try to match exactly the exact point location with the exact time of satellite overpass. The aerosol properties were retrieved from spectral reflectance at seven wavelength bands: 660, 870, 470, 550, 1 240, 1 640 and 2 120 nm using a retrieval algorithm that was formulated originally by Kaufman et al. (1997). A good correlation (r = 0.61) was obtained between MODIS AOT data at 870 nm and those observed with a portable ground–based sun photometer over Kuwait (Sabbah, 2010). However the AOT values observed on land are higher than those retrieved by MODIS–TERRA satellite. This is because the ground observations are affected by local pollution more than MODIS retrievals over open water. Daily meteorological parameters were obtained from NOAA: http://cdo.ncdc.noaa.gov/ CDO/dataproduct.

3. Monthly Variation

We calculated the monthly mean values of AOT data retrieved over Kuwait with MODIS 870 nm channel are plotted in Figure 1a during the interval from February 2000 through February 2007. Figure 1b shows those of the Angstrom wavelength exponent (α).We use a total of 85 months of data. The number of days used in each month are shown in Figure 1e. We see that the values of AOT in Figure 1a and those of the Angstrom wavelength the exponent in Figure 1b exhibit a one–year cycle variation: AOT decreases to reach a minimum around January (indicated by vertical dashed lines) and then increases to maximum around May (indicated by vertical solid lines). The reverse is true for the exponent α: It reaches the highest value around January and lowest value around May, indicating the presence of dust. The lowest values of the exponent α occurred in May–July 2005 and August 2006.

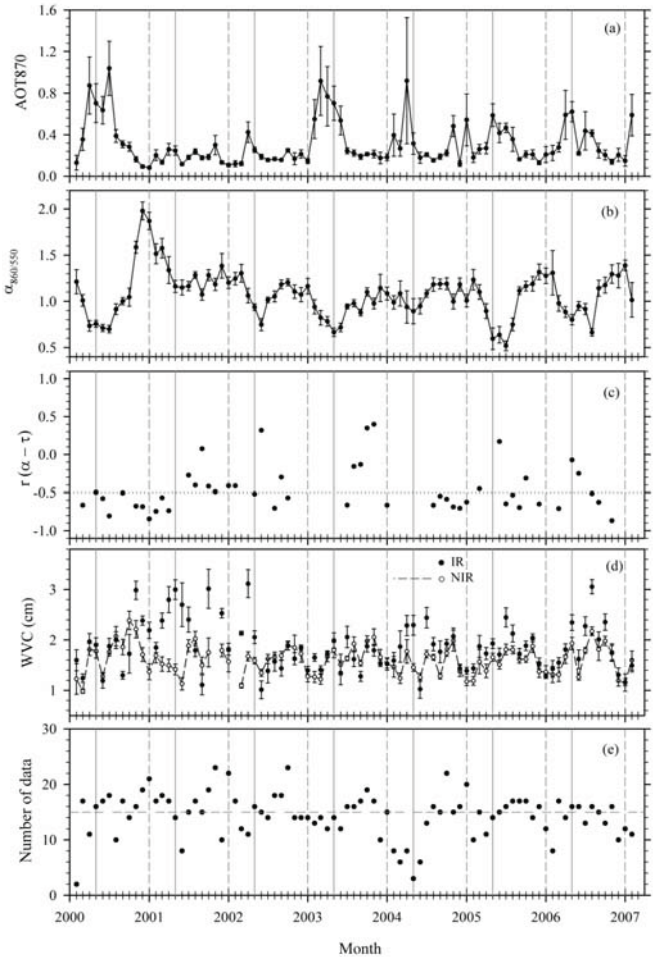

Figure 1. *Time series of the monthly mean values of:* ***(a)*** *AOT at 870 nm,* ***(b)*** *Angstrom exponent,* ***(c)*** *correlation coefficients between the daily values of AOT and α for the months with ≥15 days of data,* ***(d)*** *water vapor content observed at IR (closed circles) and NIR (open circles),* ***(e)*** *number of days used in each year. Vertical solid lines represent the month of Mays, while vertical dashed lines represent the month of Januarys.*

Sabbah et al. (2001) found a high correlation between the Angstrom exponent and AOT, indicating high dust concentration. In Figure 1c, we examine the linear correlation between the daily values of AOT and the exponent α for each month. The correlation coefficients (closed circles) in Figure 1c are calculated only for months with at least 15 days of daily mean data. We obtained 48 months with more than 15 days of daily means. We see from

Figure 1c that 31 months have a good negative correlation coefficient (r≥0.5, below the dotted line).

We plot in Figure 1d the monthly mean of water vapor content (*WVC*) observed in the IR and near–infrared (NIR) regions and in Figure 2 the mean monthly values of the meteorological parameters. We plot these parameters in order to study the climatology of the dust AOT and its relationship to the presence of water vapor in the atmosphere. MODIS is the first space instru–ment to use NIR bands together with the traditional IR bands to retrieve total precipitable water. The Level 2 precipitable water product were generated at the 1 km spatial resolution during the day, and at 5 × 5 1 km pixel resolution both day and night (Gao and Kaufman, 1998).

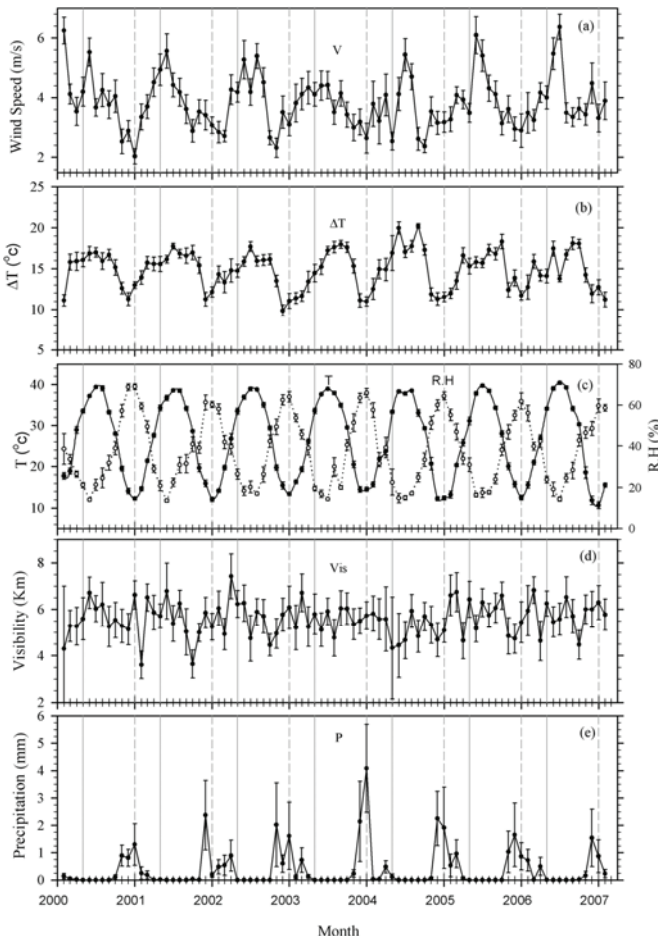

Figure 2. *Same as Figure 1 but for:* ***(a)*** *Wind speed,* ***(b)*** *the diurnal tempera–ture range,* ***(c)*** *air temperature (solid circles) and relative humidity (open circles),* ***(d)*** *visibility, and* ***(e)*** *precipitation.*

The daily mean values of the meteorological data were considered in Figure 2 for only days with AOT observations. We see that the mean monthly values of wind speed *V* were high during months with low values of the exponent *α* (June–July). The highest values of the wind speed (Figure 2a) occurred on June 2006 and July 2007. We see that the values of the diurnal temperature range *ΔT* presented in Figure 2b were high during May–July when the values of the exponent *α* were the lowest. The monthly mean values of the visibility (*Vis*) are plotted in Figure 2d while those of the precipitation (*P*) are plotted in Figure 2e. Note that we used all of the daily data in order to calculate the mean monthly values of the precipitation, as there is no much rain in Kuwait. *P* is high around January, indicated by vertical dashed line.

Table 1 shows correlation coefficients and the best fit linear equations between the monthly mean values of the coupled para–meters for the 48 months with more than 15 daily averages of data. The negative correlation between the exponent *α* and wind speed suggest that fast wind speed is associated with low *α* (dust). Dust is associated with low *RH* as *α* is positively correlated with *RH*. It is associated with high temperature as *α* is negatively correlated with the air temperature. This concludes that fast wind and dry air during summer (high temperature) helps in stirring and trans–porting dust. In contrast, Sabbah and Hassan (2008) found a negative correlation between the exponent *α* and relative humidity over Riyadh, Saudi Arabia. This may be due to growth in the size of aerosol caused by swelling moisture from air.

Table 1. *Best fit linear representations*

Parameters	r	Linear Equation
Angstrom exponent – AOT	–0.62	α = 1.373 – 0.996 AOT
Angstrom exponent – Wind speed	–0.57	α = 1.766 – 0.180 V
Angstrom exponent – Relative humidity	0.68	α = 0.666 + 0.0120 R.H
Angstrom exponent – Atmospheric temperature	–0.60	α = 1.616 – 0.0183 T
Atmospheric temperature – Relative humidity	–0.64	T = 47.864 – 0.544 R.H
Wind speed – Relative humidity	–0.73	V = 5.177 – 0.0404 R.H

3.1. Spectral analysis

Here we use fast Fourier transform (FFT) algorithms to determine Power spectral density (PSD) for monthly mean values of aerosol and meteorological parameters. Mathematical expres–sions of PSD that have been used in this study are available in Georgoulias and Kourtidis (2011). Periodic features (Sabbah and Kudela, 2011) in all the parameters are presented in Figure 3. The first harmonic of the annual cycle of all the parameters is present near the vertical solid line (denoting 12 months). The second (6–month), third (4–month) and fourth (3–month) harmonics of the annual variation (indicated by vertical dashed lines) are occasionally present. The fourth harmonic is well defined in *WVC* (NIR) spectra plotted in Figure 3a.

Williamson et al. (2010), found that the velocity components of the atmospheric wind have a PSD with a slope of –5/3 versus frequency (c/s). They found also that the atmospheric temperature and humidity have a –5/3 slope relatively as they have small direct effect on the winds. They obtained a slope of –7/6 for the aerosol particle counts PSD. A –5/3 slope in the PSD has been observed for atmospheric aerosol backscatter using LIDAR measurements (Radkevich et al., 2007). The dotted straight line in each panel of Figure 3 represent the best fit power law (t^{-n}) between PSD and the period *t* (month) during the period 2–12 months (Sabbah and Duldig, 2007). We see that the exponent *α* in Figure 3c has a steep PSD gradient with a slope of ~1.9 in the time range (2–12 months). We calculated the slope of the PSD from the monthly mean observation, while Williamson et al. (2010) calculated it from observations per second. Similarly the diurnal temperature range (*ΔT*) and the relative humidity (*RH*) in Figure 3a and b have a slope of ~1.9 in this time range. This indicates that the fluctuations in their spectra are related. The PSDs of AOT and *WVC*, exhibit a slope of ~0.7, while *V* and *Vis* have a slope of ~0.9.

3.2. Cross–correlation function

Here we preformed the cross–correlation analysis as it provides correlations between two time series in which the observations of one data series are correlated with the obser–vations of another data series at various lags and leads. Following Chatfield (1975), the cross–correlation coefficient between monthly averaged values of the Angstrom wavelength exponent *α*

and those of each of the meteorological parameter data sets (*Y*) is defined as:

$$r_{AY}(t)=\frac{C_{AY}(t)}{\sqrt{C_{AA}(0)\,C_{YY}(0)}} \qquad [t=0,\pm1,\pm2,....,\pm(N-1)] \tag{1}$$

where *N* is the series length, the cross– covariance function is given by:

$$C_{AY}(t)=\frac{1}{N}\sum_{K=1}^{N-t}\left(\alpha_K-\overline{\alpha}\right)\left(Y_{K+t}-\overline{Y}\right) \qquad [t=0,1,2,....,(N-1)]$$
$$C_{AY}(t)=\frac{1}{N}\sum_{K=1-t}^{N-t}\left(\alpha_K-\overline{\alpha}\right)\left(Y_{K+t}-\overline{Y}\right) \qquad [t=-1,-2,....,-(N-1)] \tag{2}$$

where $C_{AA}(0)$and $C_{YY}(0)$ are the sample variances of α_k and Y_k.

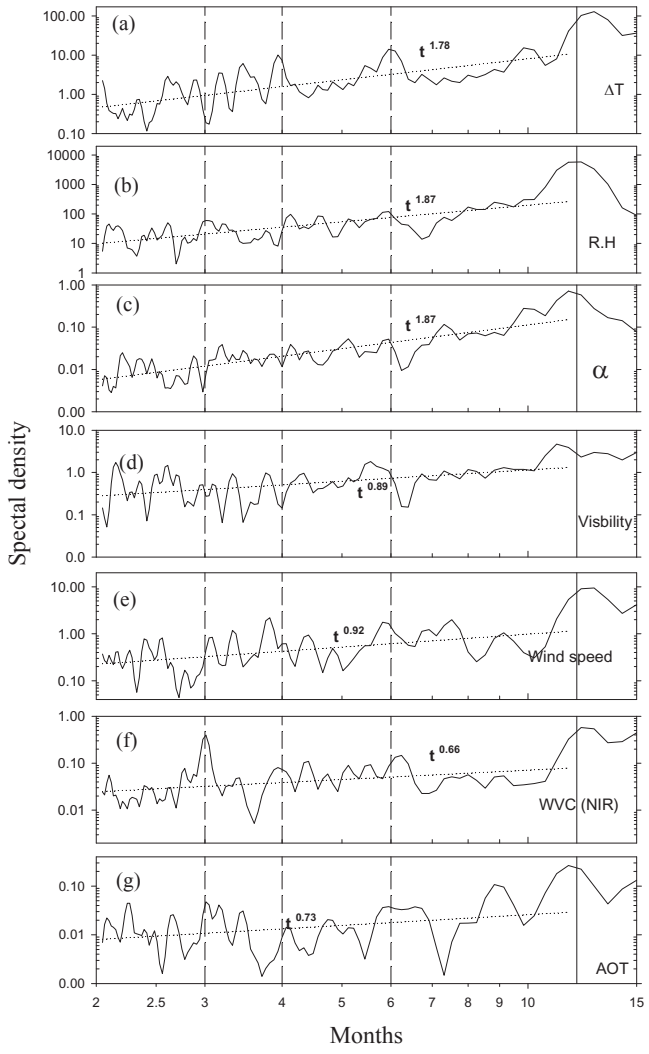

Figure 3. *Power spectral density of the monthly mean values of the aerosol and meteorological parameters during the 7 year period from 2000 through 2007. Note the annual variation of the spectra (marked with solid vertical line). The best fit for the spectra (t^{-n}) is shown for the 2–12 months period.*

Each of the meteorological data sets (*Y*) is shifted forward (or backward) by a step of one month at the time with respect to the exponent *α* and then the correlation coefficient between both data sets was calculated after each shift (Sabbah et al., 2006; Sabbah and Rybansky, 2006). In Figure 4, we plot the cross–correlation coefficient (*CCC*) between the monthly averages of the exponent *α* and those of each of the other parameters monthly averages for various time lags (0, ± 1, ± 2,....., ± 15 month). We see form Figure 4 that the time between the two maxima of the CCF (*α–V*) indicated by the upward arrows around the zero lag (Figure 4a) or that between the two minima of the CCF (*α–RH*) indicated by the downward arrows (Figure 4d) makes ∼1 year cycle. The time between the two minima of *α–V* indicated by the downward arrows (Figure 4a),or that between the two maxima of *α–RH* indicated by the upward arrows (Figure 4d) makes ∼ biennial cycle. It is also clear from Figure 4 that the CCF between *α* and any of the solar parameters display annual as well as quasi–biennial cycles. The time lag is considered at the point where the highest corre–lation between two data series is detected. Figure 4a shows that the monthly averaged values of the exponent *α* are linearly (as there is no time lag) and negatively correlated with those of the wind speed (CCC = –0.44 at zero time lag). In other words, the values of *α* reached minima (indicating the presence of dust) when the wind speed peaks (in spring and summer). The exponent *α* is linearly and negatively correlated with AOT (CCC = –0.65 at zero time lag) as well (Figure 4b). Figure 4c shows that *ΔT* is negatively correlated with the exponent *α* at –1 month time lag (*ΔT* lags the exponent *α* by one month). This means that the exponent *α* peaks (dust free) one month before *ΔT* reaches the lowest value. In contrast, Sabbah and Hassan (2008) found that the exponent *α* is correlated (r = 0.77) with the *ΔT* over the Solar Village (non coastal city). Figure 4d shows that the exponent *α* is correlated with the relative humidity (CCC = 0.61, at –1 month time lag). This can be explained as *RH* peaks (in February) one month after the exponent *α* does (one month after the atmosphere is free from dust). This also contradicts the results of the non coastal climate over the Solar Village as the exponent *α* was negative correlated (r = – 0.74) with relative humidity. Figure 4e shows that water vapor content in the NIR region is correlated with the exponent *α* (CCC = 0.49, at 3 month time lag). The atmosphere is relatively dust free (maximum value of *α*) 3 months after *WVC* peaks. Although the values of the cross correlation function between the exponent *α* and visibility shown in Figure 4f are low, they still show yearly and two–yearly cycles.

4. Seasonal Variation

Figures 5, 6 and 7 present histograms of the frequency of occurrence of the daily values of AOT, exponent *α*, *WVC* (IR and NIR), air temperature *T*, diurnal temperature range, wind speed, relative humidity and visibility for each season during the whole 7–years (2000–2007). The number of days used in each season is shown in the top of each histogram. Mean and modal values are also shown for each parameter. Inspection of Figure 5a shows a shift towards lower modal values of AOT as we go from spring to winter (right). The width of the histograms decreases as well. The reverse is true for the exponent *α* shown in Figure 5b: a shift towards higher modal values is present as we go from spring to winter. This increase in the modal values of the exponent *α* is associated with a decrease in the relative frequency of occurrence of days with low values of the exponent *α* and increase in the relative frequency of occurrence of days with high values of the *α*.

The spring (April–May) is characterized by dusty aerosols as the modal value of *α* is the lowest (∼0.81). This value seems to be high for dust. This is because MODIS tends to overestimate *α* (Levy et al., 2003). In the other hand, winter (December–March) is rather dust free with the widest histogram and largest mean value. The AOT probability distribution was the narrowest in autumn with a modal value of ∼0.12, while that of the exponent *α* was high (∼1). The most probable values of the *WVC* in the IR and NIR regions were high during summer and autumn and low during spring (Figures 5c and 6a). The modal value of the surface wind speed was

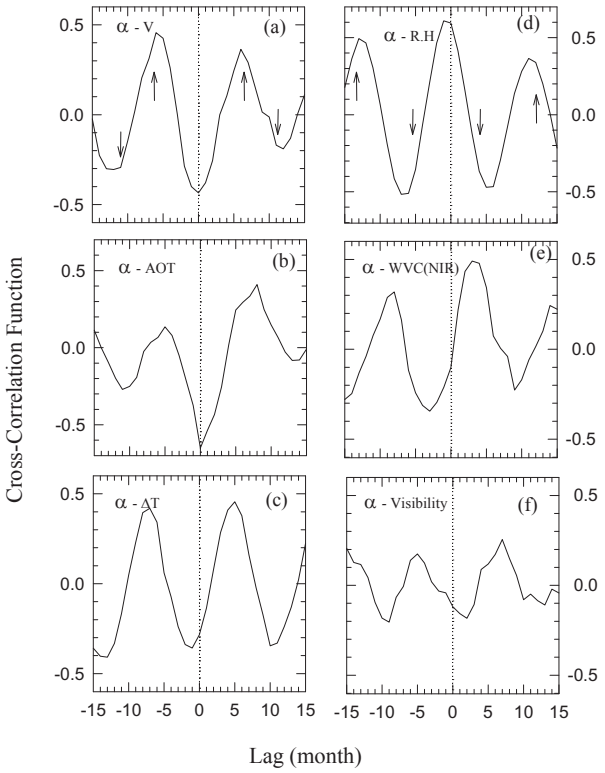

Figure 4*. Cross–correlation functions versus time lag between the Angstrom exponent α and:* ***(a)*** *wind speed, V;* ***(b)*** *AOT* ***(c)*** *diurnal temperature range, ΔT* ***(d)*** *relative humidity, RH;* ***(e)*** *water vapor content, WVC observed at NIR;* ***(f)*** *visibility.*

the highest during spring (Figure 7a). This is coinciding with the highest modal value of AOT and the lowest values of exponent *α*, *WVC* for IR and NIR regions and relative humidity (Figure 7b). The seasonal mean values of the exponent *α* are negatively correlated (r = –0.74) with those of wind speed. Using back trajectories Saeed, and Al–Dashti, (2010) showed that air masses ending in Kuwait originated from the northwestern region of the Arabian Peninsula. The major dust wind direction was northwesterly. They found that one set of trajectories moved across the northern region of the Arabian Peninsula into Kuwait and the other set of trajectories moved into the southeastern side of the Arabian Peninsula and then turned northerly converging over Kuwait from its southern borders.

The mean values of air temperature, the diurnal temperature range and wind speed were the highest in summer (June–September) during the southwest monsoon. Further the modal value of the exponent *α* was ~0.92 and the wind direction was predominantly northwesterly during summer. During autumn (October–November) the modal value of the exponent *α* increased slightly to ~1.0 while the mean value of the wind speed reached the lowest values. During winter, the northwest monsoon occurs and the modal values of AOT, *WVC*, air temperature and the diurnal temperature range was the lowest, while that of the relative humidity was the highest.

Figure 8 displays the frequency distribution (vertical bars) of the surface wind directions blowing over Kuwait, N (north), NW (north–west), W (west), SW (south–west), S (south), SE (south–east), E (east) and NE (north–east). It is clear from Figure 8 that the northwesterly "Shamal" wind direction is the most dominant. The mean values of AOT (closed circles) and those of the Angstrom exponent (open circles) are superimposed in each panel of Figure 8 for each wind direction. Error estimate of each mean are shown for

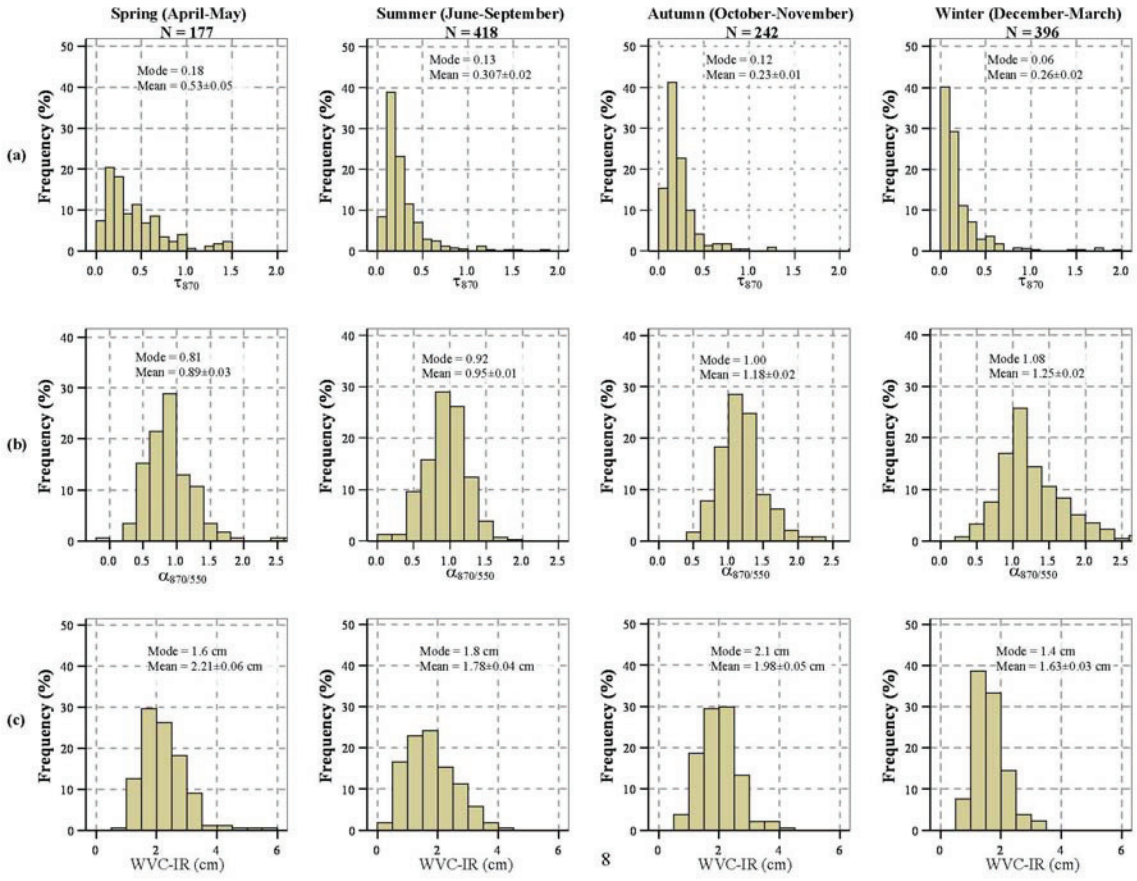

Figure 5. *Seasonal variation of the frequency distributions of:* ***(a)*** *AOT at 870 nm,* ***(b)*** *Angstrom exponent,* ***(c)*** *water vapor content (IR). Mean, modal values and the number of days are shown for each season.*

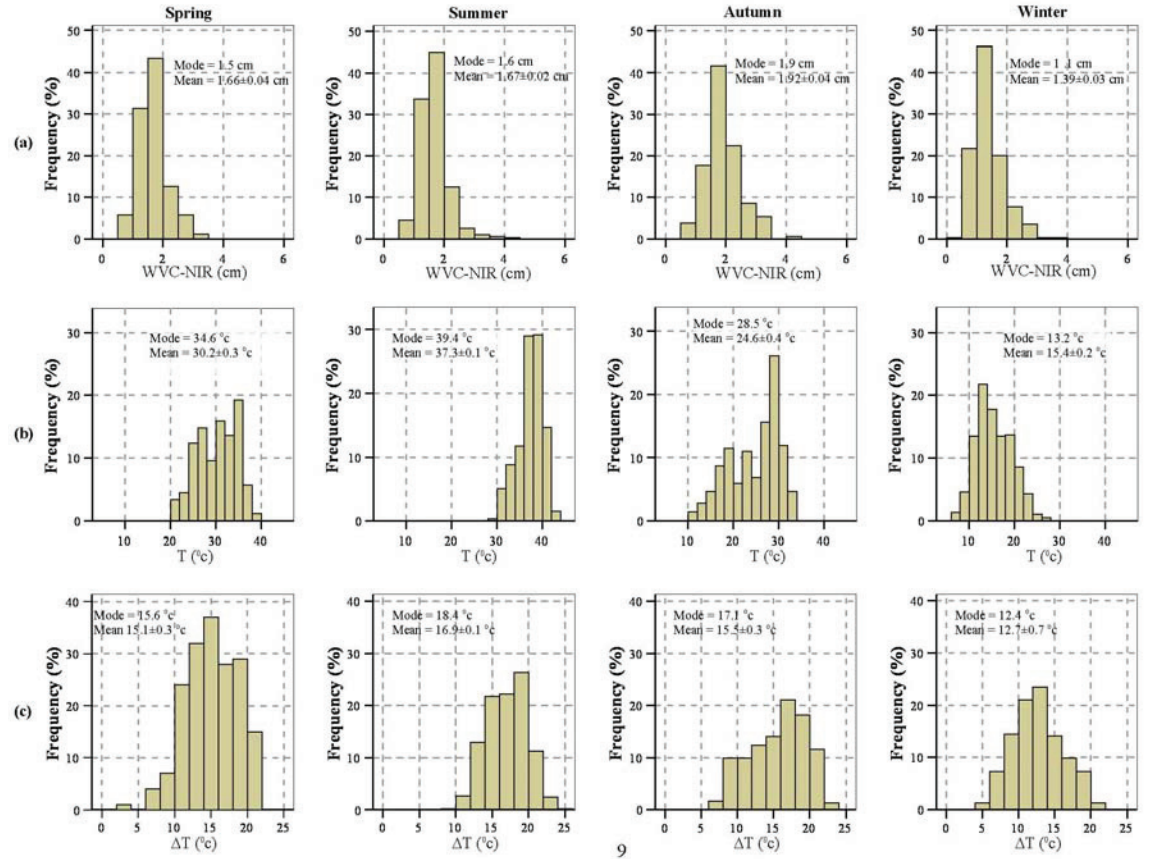

Figure 6. *Same as for Figure 4 but for:* ***(a)*** *water vapor content (NIR),* ***(b)*** *air temperature,* ***(c)*** *the diurnal temperature range.*

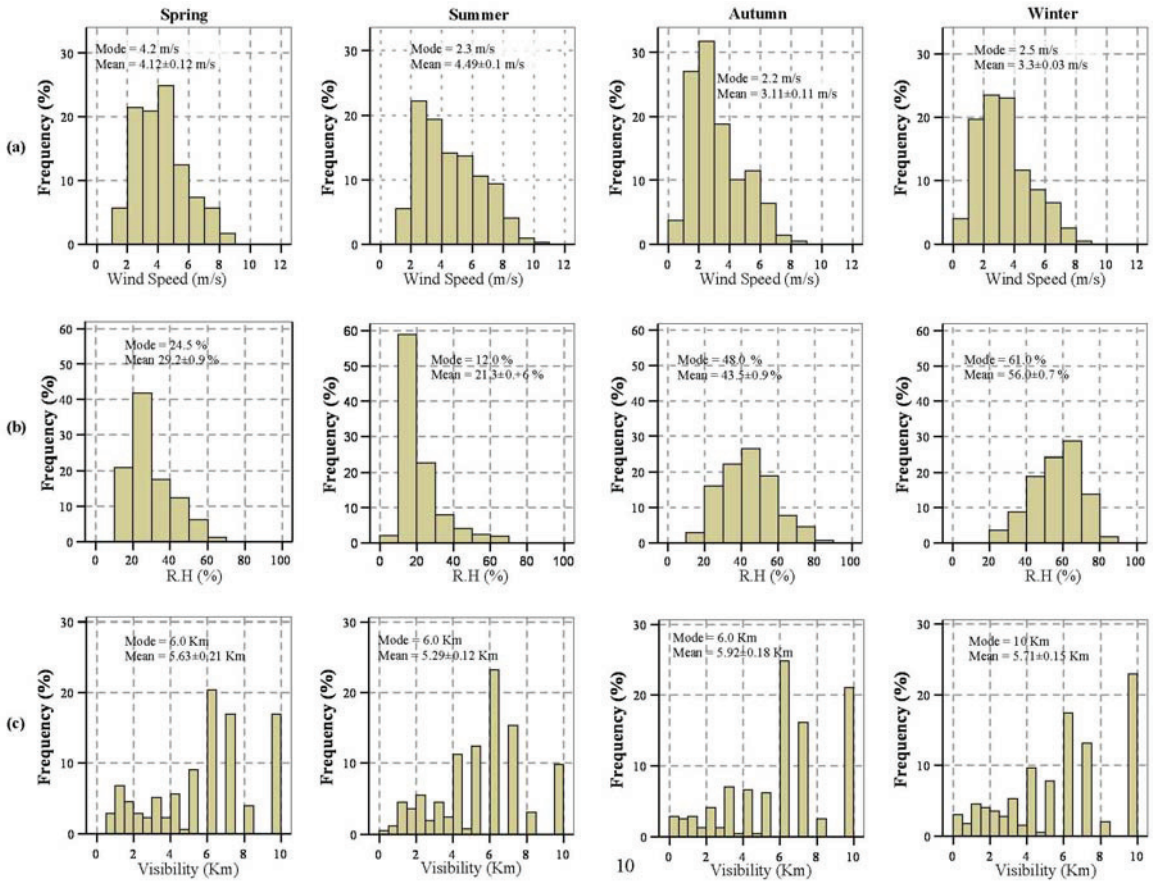

Figure 7. *Same as for Figure 4 but for:* ***(a)*** *wind speed,* ***(b)*** *relative humidity,* ***(c)*** *visibility.*

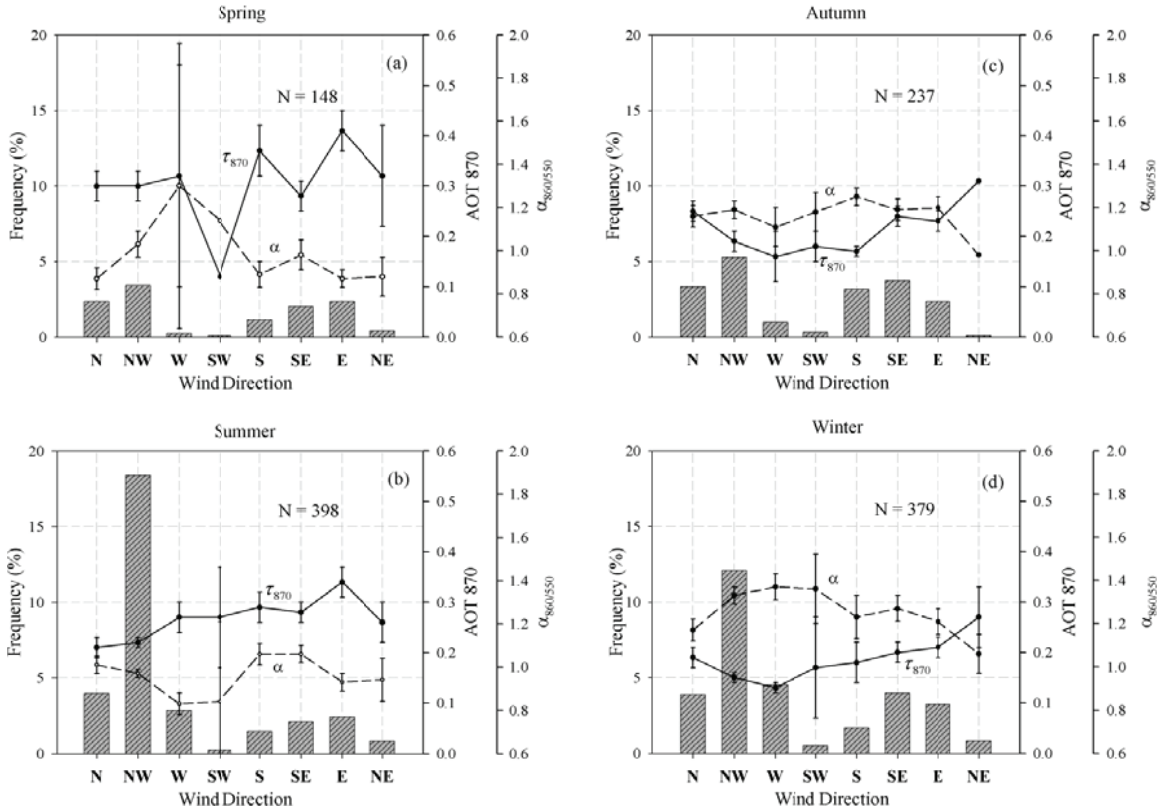

Figure 8. *The frequency distribution of wind direction blowing over Kuwait together with the associated mean values of AOT (closed circles connected with solid line), and Angstrom exponent (open circles connected with dashed line. The number of days used in each panel is indicated. Error bars represent the standard error of mean.*

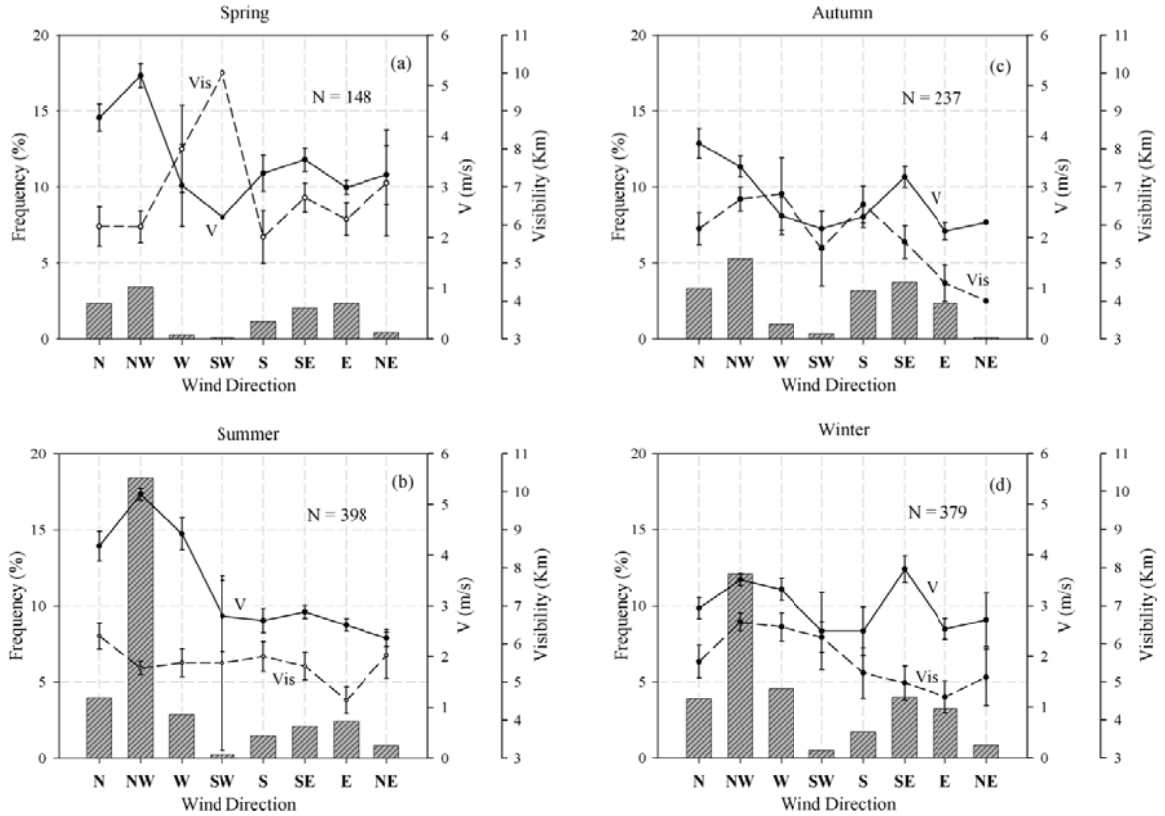

Figure 9. *Same as Figure 7 except with associated average values of the wind speed V (closed circles connected with solid line) and visibility Vis (open circles connected with dashed line).*

each parameter. We see from Figures 8a and 8b that spring and summer have lower values of the Angstrom exponent indicated by dashed lines in comparison with those in Figures 8c and 8d. These lower values of α indicate the presence of large aerosol particles (dust). The mean values of wind speed (closed circles) and those of the visibility (open circles) are shown in Figure 9 for each wind direction. We see that *V* was high when the Angstrom exponent (Figures 8a and 8b) and visibility was low for the north westerly winds during spring and summer.

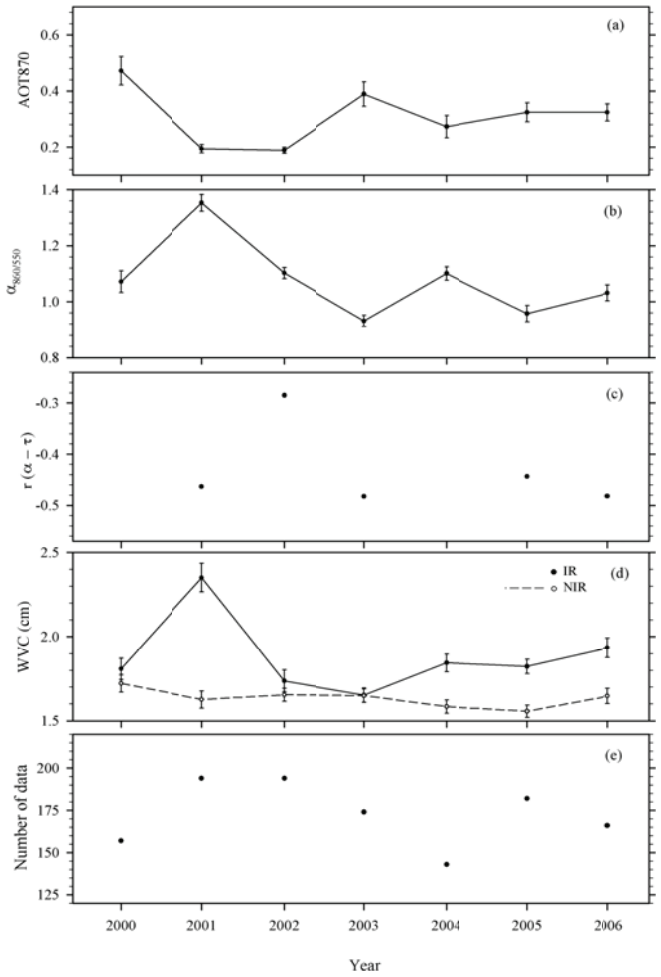

Figure 10. *Yearly mean values of:* ***(a)*** *AOT at 870 nm,* ***(b)*** *Angstrom exponent,* ***(c)*** *correlation coefficients between the yearly mean values of AOT and α* ***(d)*** *water vapor content observed at IR (closed circles) and NIR (open circles),* ***(e)*** *number of days used in each year.*

5. Yearly Variation

Figures 10 and 11 illustrate the variation in the yearly mean values of the aerosol and meteorological parameters during the 7 year interval (2000 through 2007). The yearly mean values are calculated from the daily data. The numbers of days used in each year are shown in Figure 10e. We see from Figure 10a that the value of AOT was high (0.47 ± 0.05) in 2000. It then drops significantly in 2001–2002. Next it increases to 0.39 ± 0.04 in 2003 and finally decreases to a constant value within the error bars in 2004–2006. Figure 10b shows that the annual mean value of the Angstrom exponent α was the highest (1.35 ± 0.03) in 2001 and low in 2003, 2005 and 2006. This indicates that the later three years had more dust aerosol contributions. The year 2003 had the largest dust contribution as the annual mean value of the exponent α was the lowest (0.93 ± 0.02). The annual variation in the values of α may be due to the variation of the number of occurrences and intensity of dust storms. The largest dust storms from decades occurred in Kuwait during the second Gulf War in 2003. Wilkerson (1991) reported that the likelihood of dust storms has increased by five folds since the first Gulf War. Maghrabi et al. (2011) found that March 2009 dust storm over Riyadh was one of the most intense dust storms experienced in Saudi Arabia in the last two decades.

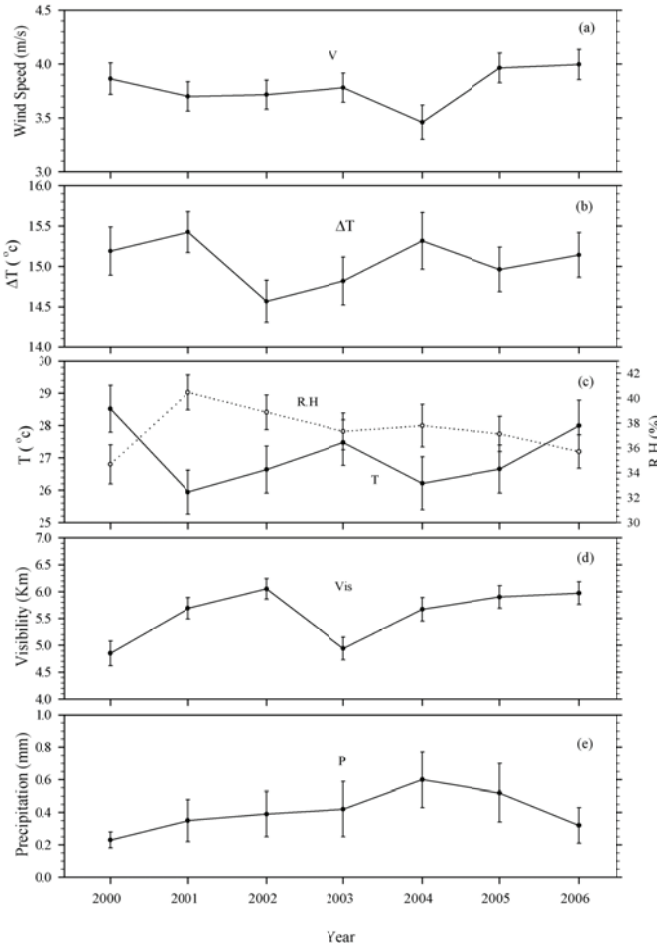

Figure 11. *Same as in Figure 10 but for:* ***(a)*** *Wind speed,* ***(b)*** *the diurnal temperature range,* ***(c)*** *air temperature (solid circles) and relative humidity (open circles),* ***(d)*** *visibility,* ***(e)*** *precipitation.*

The linear correlation coefficient between the monthly mean values of AOT and exponent α is presented in Figure 10c for each year (it is presented only for years with more than 157 days of data). We see a significant inverse correlation between the two parameters except for the year 2002. We do not see a significant variation in values of the *WVC* in the NIR region (Figure 10d). The value of the *WVC* in the IR region was low during 2000 and 2002. It increased a slightly during 2004–2006. The highest annual mean was observed in 2001.

The annual mean values of wind speed shown in Figure 11a were almost constant with the error bars. It decreased slightly in 2004. The annual mean value of ΔT (Figure 11b) was high during 2000–2001. It decreased slightly and remained constant during 2002–2006. The annual mean value of *T* was high only in 2000 and then decreased and stayed constant during 2001–2006. The reverse was true for the annual mean value of *RH* shown in Figure 11c. It was low during 2000 and then increased to a constant value during 2001–2006. The year 2003 has the highest mean values of AOT and *T* and the lowest mean value for the exponent α and visibility, if we exclude the years 2000 and 2004 with the least number of daily ≤157 days.

6. Conclusions

MODIS–TERRA satellite observations of aerosol optical depth over Kuwait were analyzed. The period of analysis includes the 7 years (2000–2007). The PSDs of the time series of the monthly mean values of AOT, exponent α and the meteorological para–meters were presented and compared in the time range 2–15 months. The annual cycle is present in the PSD of the aerosol and meteorological parameters. The second (6–month), third (4–month) and fourth (3–month) annual harmonics are evident in the PSD. The fourth harmonic is strong in *WVC* (NIR) spectra. The PSDs of the exponent α, ΔT, and *RH* increased with a similar slope of ~1.9. Spring was characterized by the high mean values of AOT, wind speed, air temperatures and water vapor content in the IR region, and low mean values of the exponent α. This implies that aerosol particles were mostly dust during the spring. The wind directions were predominantly northerly and northwesterly flowing from Iraqi deserts that bring extremely dry air and dust especially during spring. The cross–correlation analysis between the time series of the wavelength exponent and the meteorological parameters shows that the atmosphere is relatively dust free for 3 months after *WVC* (NIR) peaks. The second Gulf War year (2003) had the largest dust contribution as it has the highest mean values of AOT and air temperature and the lowest mean value for the exponent α and visibility.

Acknowledgments

The authors are grateful for the support that NASA MODIS team has provided through the online data used for this study. We also thank all anonymous reviewers for their fruitful comments and suggestions. We thank Jenan Al-Rifaai for her technical help.

References

Alpert, P., Krichak, S.O., Tsidulko, M., Shafir, H., Joseph, J.H., 2002. A dust prediction system with TOMS initialization. *Monthly Weather Review* 130, 2335-2345.

Andreae, M.O., 2001. The dark side of aerosols. *Nature* 409, 671-672.

Athar, M., Iqbal, M., Beg, M.U., Al-Ajmi, D., Al-Muzaini, S., 1998. Airborne dust collected from Kuwait in 1991-1992 augments peroxidation of cellular membrane lipids and enhances DNA, damage. *Environment International* 24, 205-212.

Bener, A., Abdulrazzaq, Y.M., Al Mutawwa, J., Debuse, P., 1996. Genetic and environmental factors associated with asthma. *Human Biology* 68, 405-414.

Chatfield, C., 1975. *The Analysis of Time Series: Theory and Practice*, Chapman and Hall, London.

Gao, B. C., Kaufman, Y. J., 1998. The MODIS Near-IR Water Vapor Algorithm, Product ID: MOD05 - Total Precipitable Water, Algorithm Technical Background Document, p.25.

Georgoulias, A.K., Kourtidis, K.A., 2011. On the aerosol weekly cycle spatiotemporal variability over Europe. *Atmospheric Chemistry and Physics* 11, 4611-4632.

Ghan, S.J., Easter, R.C., Chapman, E.G., Abdul-Razzak, H., Zhang, Y., Leung, L.R., Laulainen, N.S., Saylor, R.D., Zaveri, R.A., 2001. A physically based estimate of radiative forcing by anthropogenic sulfate aerosol. *Journal of Geophysical Research-Atmospheres* 106, 5279-5293.

Hand, J.L., Ames, R.B., Kreidenweis, S.M., Day, D.E., Malm, W.C., 2000. Estimates of particle hygroscopicity during the southeastern aerosol and visibility study. *Journal of the Air and Waste Management Association* 50, 677-685.

Haywood, J., Boucher, O., 2000. Estimates of the direct and indirect radiative forcing due to tropospheric aerosols: a review. *Reviews of Geophysics* 38, 513-543.

Hignett, P., Taylor, J.P., Francis, P.N., Glew, M.D., 1999. Comparison of observed and modeled direct aerosol forcing during TARFOX. *Journal of Geophysical Research-Atmospheres* 104, 2279-2287.

Hoff, R.M., Christopher, S.A., 2009. Remote sensing of particulate pollution from space: have we reached the promised land? *Journal of the Air and Waste Management Association* 59, 645-675.

Ichoku, C., Chu, D.A., Mattoo, S., Kaufman, Y.J., Remer, L.A., Tanre, D., Slutsker, I., Holben, B.N., 2002. A spatio temporal approach for global validation and analysis of MODIS aerosol products. *Geophysical Research Letters* 29, art. no. 1616.

Jacobson, M.Z., 2001. Global direct radiative forcing due to multicomponent anthropogenic and natural aerosols. *Journal of Geophysical Research-Atmospheres* 106, 1551-1568.

Jones, T.A., Christopher, S.A., 2008. Seasonal variation in satellite derived effects of aerosols on clouds in the Arabian Sea. *Journal of Geophysical Research-Atmospheres* 113, art. no. D09207.

Kaskaoutis, D.G., Kambezidis, H.D., Nastos, P.T., Kosmopoulos, P.G., 2008. Study on an intense dust storm over Greece. *Atmospheric Environment* 42, 6884-6896.

Kaufman, Y.J., Tanre, D., Remer, L.A., Vermote, E.F., Chu, A., Holben, B.N., 1997. Operational remote sensing of tropospheric aerosol over land from EOS moderate resolution imaging spectroradiometer. *Journal of Geophysical Research-Atmospheres* 102, 17051-17067.

Kellogg, C.A., Griffin, D.W., Garrison, V.H., Peak, K.K., Royall, N., Smith, R.R., Shinn, E.A., 2004. Characterization of aerosolized bacteria and fungi from desert dust events in Mali, West Africa. *Aerobiologia* 20, 99-110

Levy, R.C., Remer, L.A., Tanre, D., Kaufman, Y.J., Ichoku, C., Holben, B.N., Livingston, J.M., Russell, P.B., Maring, H., 2003. Evaluation of the moderate resolution imaging spectroradiometer (MODIS) retrievals of dust aerosol over the ocean during PRIDE. *Journal of Geophysical Research-Atmospheres* 108, 8594.

Maghrabi, A., Alharbi, B., Tapper, N., 2011. Impact of the March 2009 dust event in Saudi Arabia on aerosol optical properties, meteorological parameters, sky temperature and emissivity. *Atmospheric Environment* 45, 2164-2173.

Malm, W.C., Sisler, J.F., Huffman, D., Eldred, R.A., Cahill, T.A., 1994. Spatial and seasonal trends in particle concentration and optical extinction in the United States. *Journal of Geophysical Research-Atmospheres* 99, 1347-1370.

Mims, F.M., Holben, B.N., Eck, T.F., Montgomery, B.C., Grant, W.B., 1997. Smoky skies, mosquitoes, and disease. *Science* 276, 1774-1775.

Prospero, J.M., Blades, E., Mathison, G., Naidu, R., 2005. Interhemispheric transport of viable fungi and bacteria from Africa to the Caribbean with soil dust. *Aerobiologia* 21, 1-19.

Prospero, J.M., 1999. Long-term measurements of the transport of African mineral dust to the southeastern United States: implications for regional air quality. *Journal of Geophysical Research-Atmospheres* 104, 15917-15927.

Prospero, J.M., Carlson, T.N., 1972. Vertical and areal distribution of Saharan dust over the western equatorial North Atlantic Ocean. *Journal of Geophysical Research* 77, 5255–5265.

Radkevich, A., Lovejoy, S., Strawbridge, K., Schertzer, D., 2007. The elliptical dimension of space time atmospheric stratification of passive admixtures using lidar data. *Physica A-Statistical Mechanics and Its Applications* 382, 597-615.

Ramanathan, V., Crutzen, P.J., Kiehl, J.T., Rosenfeld, D., 2001. Atmosphere - aerosols, climate, and the hydrological cycle. *Science* 294, 2119-2124.

Redemann, J., Zhang, Q., Schmid, B., Russell, P.B., Livingston, J.M., Jonsson, H., Remer, L.A., 2006. Assessment of MODIS derived visible and near-IR aerosol optical properties and their spatial variability in the presence of mineral dust. *Geophysical Research Letters* 33, art. no. L18814.

Rosenfeld, D., 2000. Suppression of rain and snow by urban and industrial air pollution. *Science* 287, 1793-1796.

Sabbah, I., Kudela, K., 2011. Third harmonic of the 27-day periodicity of galactic cosmic rays - coupling with interplanetary parameters. *Journal of Geophysical Research* 116, art. no. A04103.

Sabbah, I., 2010. Impact of aerosol on air temperature in Kuwait. *Atmospheric Research* 97, 303-314.

Sabbah, I., Hasan, F.A., 2008. Remote sensing of aerosols over the solar village, Saudi Arabia. *Atmospheric Research* 90, 170-179.

Sabbah, I., Duldig, M.L., 2007. Solar polarity dependence of cosmic ray power spectra observed with MAWSON underground MUON telescopes. *Solar Physics* 243, 231-235.

Sabbah, I., Rybansky, M., 2006. Galactic cosmic ray modulation during the last five solar cycles. *Journal of Geophysical Research-Space Physics* 111, art. no. A01105.

Sabbah, I., Saeed, T., Al-Jassar, H., Rao, K.S., 2006. Remote sensing of desert dust in Kuwait. *Kuwait Journal of Science and Engineering* 33, 101-117.

Sabbah, I., Ichoku, C., Kaufman, Y.J., Remer, L., 2001. Full year cycle of desert dust spectral optical thickness and precipitable water vapor over Alexandria, Egypt. *Journal of Geophysical Research-Atmospheres* 106, 18305-18316.

Saeed, T.M., Al-Dashti, H., 2011. Optical and physical characterization of "Iraqi freedom" dust storm, a case study. *Theoretical and Applied Climatology* 104, 123-137.

Samet, J.M., Dominici, F., Curriero, F.C., Coursac, I., Zeger, S.L., 2000. Fine particulate air pollution and mortality in 20 US cities, 1987-1994. *New England Journal of Medicine* 343, 1742-1749.

Ulanowski, Z., Sabbah, I., Harrison, R.G., Nicoll, K.A., Hirst, E., Kaye, P.H., Al-Abbadi, N., Rogers, G., 2010. Atmospheric dust charging, vertical profiles and optical properties measured in the Arabian Peninsula during the DREAME campaign. *EGU General Assembly* 12, EGU2010-13473.

Watson, J.G., 2002. Visibility: science and regulation. *Journal of the Air and Waste Management Association* 52, 628-713.

Wilkerson, W.D., 1991. Dust and Sand Forecasting in Iraq and Adjoining Countries, AWS/TN-91/001, Air Weather Services, Scott Air Force Base, Illinois 62225-5008.

Williamson, C.C., Hill, S.C., Garvey, D.M., Larsen, M.L., Klipp, C.L., 2010. Power Spectral Densities of Atmospheric Aerosol Particle Counts, ARL-TR-5064, Army Research Laboratory, Adelphi, MD 20783-1197.

Xia, X.A., Chen, H.B., Wang, P.C., Zhang, W.X., Goloub, P., Chatenet, B., Eck, T.F., Holben, B.N., 2006. Variation of column-integrated aerosol properties in a Chinese urban region. *Journal of Geophysical Research-Atmospheres* 111, art. no. D05204.

Yu, H., Kaufman, Y.J., Chin, M., Feingold, G., Remer, L.A., Anderson, T.L., Balkanski, Y., Bellouin, N., Boucher, O., Christopher, S., DeCola, P., Kahn, R., Koch, D., Loeb, N., Reddy, M.S., Schulz, M., Takemura, T., Zhou, M., 2006. A review of measurement based assessments of the aerosol direct radiative effect and forcing. *Atmospheric Chemistry and Physics* 6, 613-666.